Improved cosmological fits with quantized primordial power spectra

D. J. Bartlett[1,2,3,4,*] W. J. Handley[1,5,6,†] and A. N. Lasenby[1,5,‡]

[1]*Astrophysics Group, Cavendish Laboratory,*
J.J. Thomson Avenue, Cambridge, CB3 0HE, United Kingdom
[2]*Trinity College, Trinity Street, Cambridge, CB2 1TQ, United Kingdom*
[3]*Astrophysics, University of Oxford,*
Denys Wilkinson Building, Keble Road, Oxford, OX1 3RH, United Kingdom
[4]*Oriel College, Oriel Square, Oxford, OX1 4EW, United Kingdom*
[5]*Kavli Institute for Cosmology, Madingley Road, Cambridge, CB3 0HA, United Kingdom*
[6]*Gonville & Caius College, Trinity Street, Cambridge, CB2 1TA, United Kingdom*

We observationally examine cosmological models based on primordial power spectra with quantized wave vectors. Introducing a linearly quantized power spectrum with $k_0 = 3.225 \times 10^{-4}$ Mpc^{-1} and spacing $\Delta k = 2.257 \times 10^{-4}$ Mpc^{-1} provides a better fit to the *Planck* 2018 observations than the concordance baseline, with $\Delta\chi^2 = -8.55$. Extending the results of Lasenby *et al.* [preceding paper, Perturbations and the future conformal boundary, Phys. Rev. D **105**, 083514 (2022)], we show that the requirement for perturbations to remain finite beyond the future conformal boundary in a universe containing dark matter and a cosmological constant results in a linearly quantized primordial power spectrum. It is found that the infrared cutoffs for this future conformal boundary quantized cosmology do not provide cosmic microwave background power spectra compatible with observations, but future theories may predict more observationally consistent quantized spectra.

I. INTRODUCTION

There has been much historical discussion of the significance of low-multipole features in the cosmic microwave background power spectrum [1–3], with many proposed primordial mechanisms to explain these features with varying degrees of naturalness [4]. In a recent paper, Lasenby *et al.* [5] proposed a novel mechanism for setting initial conditions on cosmological perturbations derived from considerations of the future conformal boundary in radiation dominated universes. The key prediction of this theory is a quantization of wave vectors for the primordial power spectrum of curvature perturbations. These quantized primordial spectra are capable of generating features in the cosmic microwave background (CMB) power spectrum such as suppression of power at low multipoles, features at intermediate multipoles and oscillations at higher multipoles.

Lasenby *et al.* [5] established in detail how such quantized spectra arise through consistency considerations of a linearized treatment of perturbations, and in particular their behavior as they approach and then pass through the future conformal boundary (FCB). They also derived the evolution of particle geodesics through the FCB, and

discussed how one can interpret the nature of a universe beyond this point, and "two-sheeted universes" have been discussed by [6]. In Sec. III we fit these models to the latest *Planck* 2018 CMB data [7,8] and find that while these models produce qualitatively interesting observational features they do not provide a better fit in comparison with the ΛCDM baseline. In Sec. IV we extend the scheme and scan through a class of parametrized quantized models, and find that some models within this class provide a markedly improved fit in comparison with the ΛCDM baseline. Such models are capable of reconstructing both the suppression of power in low-multipole CMB power spectra and the $20 \lesssim \ell \lesssim 30$ dip. We conclude in Sec. V and discuss future extensions which may be able to predict *a priori* these best-fitting quantization schemes.

II. ΛCDM FCB QUANTIZATION

In Ref. [5] it was shown that for a universe with only radiation and a cosmological constant, the equations governing the background and perturbations are analytically continuable through the future conformal boundary. Making the requirement that the perturbative expansion remains finite throughout the domain results in there being only a discrete set of wave vectors that are allowed.

Lasenby *et al.* [5] also showed that for a universe with only matter, the equations are analytically continuable if the

[*]deaglan.bartlett@physics.ox.ac.uk
[†]wh260@mrao.cam.ac.uk
[‡]a.n.lasenby@mrao.cam.ac.uk

energy density is viewed as $\rho_{\rm m} \sim a^{-3} = s^3$. However, as s and a are negative on the other side of the future conformal boundary, this results in radically different behavior in contrast to the symmetry associated with the radiation-only case. As an alternative to this, one can define the material component as having a scaling $\rho_{\rm m} \sim |a|^{-3}$. This retains the symmetry on either side of the future conformal boundary, at the expense of analyticity since the modulus function $|s|$ is not differentiable at the FCB $s = 0$. One can however ensure that things remain physical in spite of this by requiring that energy remains continuous for both the background and perturbations, which is shown to be equivalent to requiring that the solutions are symmetric or antisymmetric about the future conformal boundary.

In this section, we consider universes with a cosmological constant alongside both noninteracting material and radiative components as an approximation to the concordance ΛCDM cosmology. As in Ref. [5], we start by approximating these components as perfect fluids and later consider the impact of higher-order multipoles in the Boltzmann hierarchy. However, unlike in Ref. [5], the equations for the combined case are not analytically solvable, so we must proceed using series expansion techniques.

A. Background equations

Throughout this paper we use units $8\pi G = c = \hbar = k_{\rm B} = 1$ and consider spatially flat universes in the Newtonian gauge with potentials Ψ, Φ such that the metric is defined by

$$g_{\mu\nu}dx^\mu dx^\nu = a^2(\eta)[(1 + 2\Psi)d\eta^2 - (1 - 2\Phi)d\vec{x}^2]. \quad (1)$$

The background evolution of a universe filled with non-interacting barotropic fluids is defined by the Friedmann equation:

$$H^2 = \frac{\dot{a}^2}{a^4} = \frac{1}{3}\sum_i \rho_i, \qquad \rho_i = 3H_0^2\Omega_i|a|^{-3(1+w_i)}, \quad (2)$$

where a is the scale factor, ρ_i is the density of the ith fluid component with equation of state parameter w_i, H_0 is the present-day value of the Hubble parameter H, Ω_i is the fractional contribution of fluid i to the universal energy budget today and derivatives with respect to conformal time are denoted with an overdot.

B. Perturbation equations

1. Perfect fluid approximation

Scalar perturbations $\delta\rho_i$ to the background densities ρ_i are defined as $\delta_i \equiv \delta\rho_i/\bar{\rho}_i$, and the peculiar velocities of these fluid perturbations are defined to be $\vec{v}_i \equiv \vec{\nabla}v_i$. To linear order, and assuming that all components are perfect fluids, the scalar perturbations evolve as [9]

$$\dot{\Phi} = -\frac{\dot{a}}{a}\Phi - \frac{1}{2}a^2\sum_i(1 + w_i)\rho_i v_i, \quad (3)$$

$$\dot{\delta}_i = (1 + w_i)(3\dot{\Phi} + v_i k^2), \quad (4)$$

$$\dot{v}_i = 3\frac{\dot{a}}{a}\left(w_i - \frac{1}{3}\right)v_i - \left(\Phi + \frac{w_i}{1 + w_i}\delta_i\right). \quad (5)$$

One can also express potentials algebraically in terms of the other components via

$$\Phi = \Psi = \frac{1}{2k^2}\sum_i\left(3\frac{\dot{a}}{a}(1 + w_i)v_i - \delta_i\right)a^2\rho_i. \quad (6)$$

We take the fluid index i to range over $i \in \{{\rm r, m}, \Lambda\}$ for radiation $w_{\rm r} = \frac{1}{3}$, matter $w_{\rm m} = 0$ and dark energy $w_\Lambda = -1$ respectively, but in general only perturb the first two of these.

It should be noted that Eqs. (1)–(6) are symmetric under the transformation $a \to -a$, $d\eta \to -d\eta$, provided that the perturbations transform as $\Phi \to \pm\Phi$ and $\delta_i \to \pm\delta_i$, $v_i \to \mp v_i$. The opposing sign of v_i is intuitive, since it is a velocity-like term that should change direction on changing the sign of $d\eta$.

2. Boltzmann hierarchy

In reality one should describe photons via a distribution function in photon momentum and not as a perfect fluid. Decomposing the perturbation to this distribution function into momentum-averaged Legendre components, $F_{{\rm r}\ell}$, and defining $G_{{\rm r}\ell}$ to be the photon polarization component, we must solve the Boltzmann hierarchy [9]

$$k^2\Phi = -\frac{1}{2}a^2\sum_i\left(\delta\rho_i + 3\frac{\dot{a}}{a}(\bar{\rho}_i + \bar{P}_i)\frac{\theta_i}{k^2}\right), \quad (7)$$

$$k^2(\Phi - \Psi) = \frac{3}{2}a^2\sum_i(\bar{\rho}_i + \bar{P}_i)\sigma_i, \quad (8)$$

$$\dot{\delta}_{\rm m} = -\theta_{\rm m} + 3\dot{\Phi}, \quad (9)$$

$$\dot{\theta}_{\rm m} = -\frac{\dot{a}}{a}\theta_{\rm m} + k^2\Psi, \quad (10)$$

$$\dot{\delta}_{\rm r} = -\frac{4}{3}\theta_{\rm r} + 4\dot{\Phi}, \quad (11)$$

$$\dot{\theta}_{\rm r} = k^2\left(\frac{\delta_{\rm r}}{4} - \sigma_{\rm r}\right) + k^2\Psi + an_{\rm e}\sigma_{\rm T}(\theta_{\rm b} - \theta_{\rm r}), \quad (12)$$

$$\dot{F}_{\rm r2} = 2\dot{\sigma}_{\rm r} = \frac{8}{15}\theta_{\rm r} - \frac{3}{5}kF_{\rm r3} - \frac{9}{5}an_{\rm e}\sigma_{\rm T}\sigma_{\rm r}$$
$$+ \frac{1}{10}an_{\rm e}\sigma_{\rm T}(G_{\rm r0} + G_{\rm r2}), \quad (13)$$

$$\dot{F}_{r\ell} = \frac{k}{2\ell+1}[\ell F_{r(\ell-1)} - (\ell+1)F_{r(\ell+1)}]$$
$$- an_e\sigma_T F_{r\ell}, \qquad \ell \geq 3, \tag{14}$$

$$\dot{G}_{r\ell} = \frac{k}{2\ell+1}[\ell G_{r(\ell-1)} - (\ell+1)G_{r(\ell+1)}]$$
$$+ an_e\sigma_T \left[\frac{1}{2}(F_{r2} + G_{r0} + G_{r2})\left(\delta_{\ell 0} + \frac{\delta_{\ell 2}}{5}\right) - G_{r\ell}\right], \tag{15}$$

where the subscript b refers to baryons, n_e is the electron number density, σ_T is the Thomson scattering cross section, and

$$\theta_i = -k^2 v_i, \qquad \sigma_i = \frac{\Pi_i}{6}, \tag{16}$$

for anisotropic stress Π_i. Once again, we consider the fluid index over the range $i \in \{r, m, \Lambda\}$ and perturb only the first two of these.

As in Ref. [5], we work in an approximation where, before recombination, there is tight coupling between matter and radiation, and therefore use the perfect fluid approximation. After recombination we assume free streaming, and therefore set $n_e = \sigma_m = 0$. We see that this decouples $G_{r\ell}$ from the other perturbations, so we do not consider these terms further.

C. Initial conditions

We may initialize the perturbation equations close to the singularity $\eta = 0$ uniquely if we select the finite perturbative modes and consider only adiabatic perturbations so that $\delta_m = \frac{3}{4}\delta_r$ and $v_m = v_r$ as $\eta \to 0$. Expanding Eqs. (4)–(6) as power series in η under these constraints yields to first order

$$\delta_r(\eta) \propto -2 - \frac{H_0\Omega_m}{4\sqrt{\Omega_r}}\eta + \mathcal{O}(\eta^2), \tag{17}$$

$$v_r(\eta) \propto -\frac{1}{2}\eta + \mathcal{O}(\eta^2), \tag{18}$$

$$\delta_m(\eta) \propto -\frac{3}{2} - \frac{3H_0\Omega_m}{16\sqrt{\Omega_r}}\eta + \mathcal{O}(\eta^2), \tag{19}$$

$$v_m(\eta) \propto -\frac{1}{2}\eta + \mathcal{O}(\eta^2), \tag{20}$$

$$\Phi(\eta) \propto 1 - \frac{H_0\Omega_m}{16\sqrt{\Omega_r}}\eta + \mathcal{O}(\eta^2), \tag{21}$$

where the proportionality constant is the same for all expressions and without loss of generality following Ref. [5] we define $\Phi = 1$ at the singularity. Although written here to first order, we evaluate the velocity perturbations to fourth order, and the overdensity and potential to third order. We find that reducing this to third and second order, respectively, does not change our results.

D. The future conformal boundary

We may now solve for the perturbations up to an arbitrary rescaling by integrating the background and perturbation equations beginning with the initial conditions (17)–(21). If we extrapolate this evolution beyond the present day, at some finite time in the conformal future we reach the future conformal boundary $\eta = \eta_\infty$. Although the scale factor diverges $a \to \infty$ as $\Delta\eta = \eta - \eta_\infty \to 0_-$, all other terms in the background and perturbation equations remain finite, and the solution may be continued beyond this boundary. By symmetry, the background solution eventually arrives at a big crunch at $\eta = 2\eta_\infty$. In order for our setup to be valid, following Ref. [5] we should also demand that our perturbation variables remain finite at all times. For a general wave vector k, this will not be true, but for a discrete spectrum of wave numbers it can be. As determined in Ref. [5], all of the technical considerations about perturbations remaining finite and analytic continuation through the future conformal boundary crystallize in practice into a symmetry requirement which we may numerically impose.

The conceptual strategy is therefore to compute the solutions of the perturbations at the future conformal boundary for each k, selecting those wave numbers whose solutions pass through the boundary with the correct symmetry (Fig. 1).

1. Perfect fluid approximation

We start by considering perturbations for a perfect fluid, where the power series solutions about the future conformal boundary of Eqs. (2)–(5) take the form

$$\delta_r = \delta_r^\infty - \frac{2}{3k^2}\left[\text{sign}(\Delta\eta) \times 9H_\infty^3\frac{\Omega_m}{\Omega_\Lambda}(\delta_m^\infty + 3\dot{v}_m^\infty) - 2\left(k^4 - 18H_\infty^4\frac{\Omega_r}{\Omega_\Lambda}\right)v_r^\infty\right]\Delta\eta + \mathcal{O}(\Delta\eta^2), \tag{22}$$

$$v_r = v_r^\infty - \frac{1}{4}\delta_r^\infty \Delta\eta + \mathcal{O}(\Delta\eta^2), \tag{23}$$

$$\delta_m = \delta_m^\infty - \frac{9}{2k^2}\left[\text{sign}(\Delta\eta) \times H_\infty^3\frac{\Omega_m}{\Omega_\Lambda}(\delta_m^\infty + 3\dot{v}_m^\infty) + 4H_\infty^4\frac{\Omega_r}{\Omega_\Lambda}v_r^\infty\right]\Delta\eta + \mathcal{O}(\Delta\eta^2), \tag{24}$$
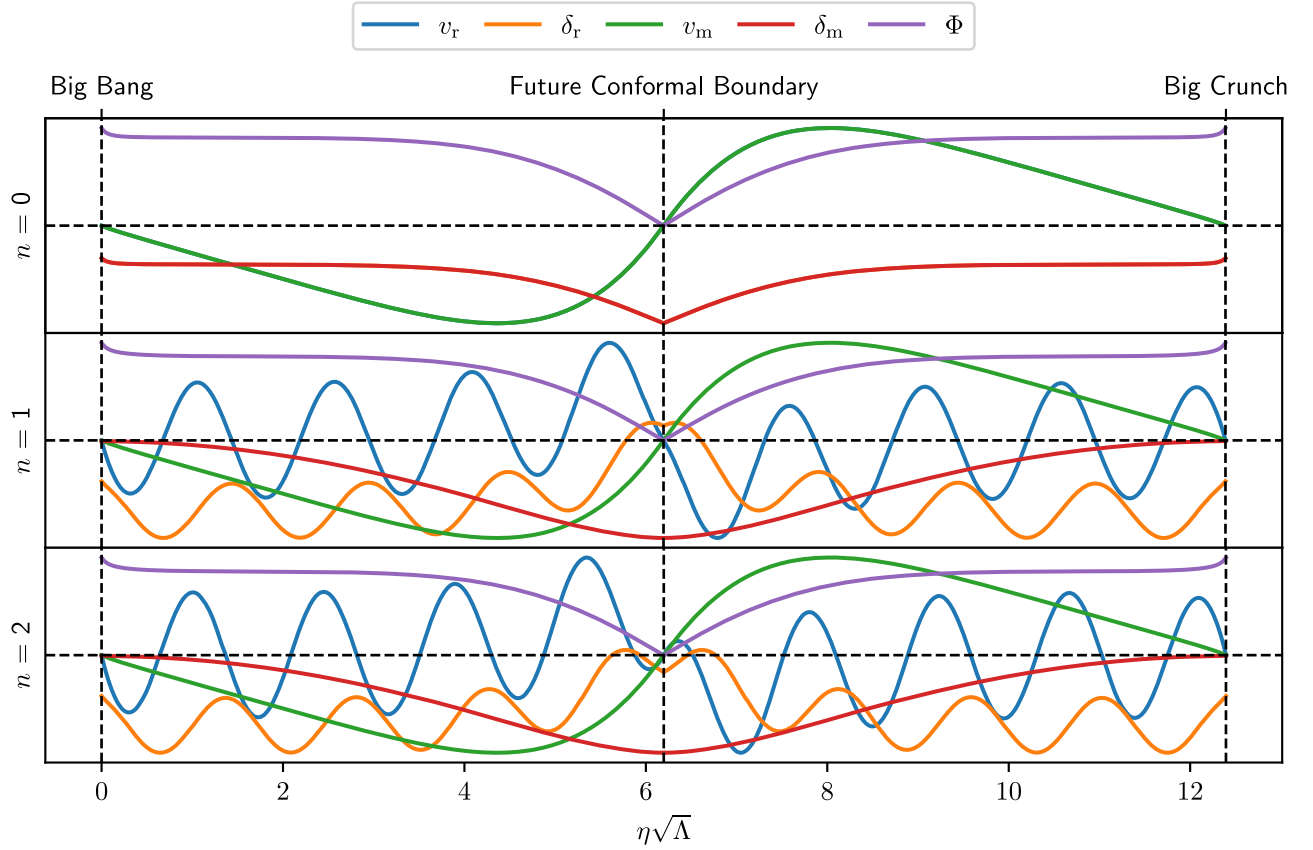
FIG. 1. Radiation, matter and potential perturbations for the first three solutions which remain finite on both sides of the future conformal boundary in a ΛCDM universe containing only perfect fluids with cosmological parameters set to the *Planck* 2018 best-fit values.

$$v_{\mathrm{m}} = \dot{v}_{\mathrm{m}}^{\infty} \Delta\eta + \mathcal{O}(\Delta\eta^2), \tag{25}$$

$$\Phi = -\frac{3}{2k^2}\left[\mathrm{sign}(\Delta\eta) \times H_{\infty}^3 \frac{\Omega_{\mathrm{m}}}{\Omega_{\Lambda}}(\delta_{\mathrm{m}}^{\infty} + 3\dot{v}_{\mathrm{m}}^{\infty}) + 4H_{\infty}^4 \frac{\Omega_{\mathrm{r}}}{\Omega_{\Lambda}}v_{\mathrm{r}}^{\infty}\right]\Delta\eta + \mathcal{O}(\Delta\eta^3), \tag{26}$$

where the Hubble constant at the future conformal boundary is calculated as $H_{\infty} = H_0\sqrt{\Omega_{\Lambda}}$.

The four variables $\{v_r^{\infty}, \delta_{\mathrm{r}}^{\infty}, \dot{v}_{\mathrm{m}}^{\infty}, \delta_{\mathrm{m}}^{\infty}\}$ are the leading terms in each solution's power series expansion, determine the higher order terms in the series and are themselves determined up to an overall scaling by integrating Eqs. (2)–(5) up to η_{∞} beginning with the initial conditions (17)–(21), and can be viewed therefore as functions of k. For continuity, $\{v_{\mathrm{r}}^{\infty}, \delta_{\mathrm{r}}^{\infty}, \delta_{\mathrm{m}}^{\infty}\}$ take the same value either side of the future conformal boundary; however this is not necessarily true for $\dot{v}_{\mathrm{m}}^{\infty}$ as the derivative of v_{m} could be discontinuous.

Equation (23) is critical, as we can only have antisymmetry in v_r if $v_r^{\infty} = 0$. Assuming this is not true, we would require that the term depending on the sign of $\Delta\eta$ in Eq. (24) is the same on either side of the future conformal boundary, since this is added to a term proportional to v_{r}^{∞}, which does not change sign. For this to be true, we require

$$\delta_{\mathrm{m}}^{\infty} = -\frac{3}{2}[\dot{v}_{\mathrm{m}}^{\infty}(\Delta\eta > 0) + \dot{v}_{\mathrm{m}}^{\infty}(\Delta\eta < 0)], \quad \text{if } v_{\mathrm{r}}^{\infty} \neq 0. \tag{27}$$

We find that we always have a finite δ_{m} at the future conformal boundary and therefore δ_{m} is required to be symmetric about this point. This is equivalent to requiring the linear term in Eq. (24) to change sign; hence

$$8H_{\infty}\Omega_{\mathrm{r}}v_{\mathrm{r}}^{\infty} = -3\Omega_{\mathrm{m}}[\dot{v}_{\mathrm{m}}^{\infty}(\Delta\eta > 0) - \dot{v}_{\mathrm{m}}^{\infty}(\Delta\eta < 0)]. \tag{28}$$

Solving for $\dot{v}_{\mathrm{m}}^{\infty}$ on either side of the future conformal boundary and substituting into Eq. (24), we obtain

$$v_m = -\frac{1}{3}\left(\delta_m^\infty + \text{sign}(\Delta\eta) \times 4H_\infty \frac{\Omega_r}{\Omega_m} v_r^\infty\right)\Delta\eta + \mathcal{O}(\Delta\eta^2).$$ (29)

We have assumed $v_r^\infty \neq 0$ and used $\delta_m^\infty \neq 0$ but, if both of these are true, the above expression means we cannot make v_m either symmetric or antisymmetric about the future conformal boundary and we thus arrive at a contradiction. The only allowed modes are those where $v_r^\infty = 0$. We note that in this case $\dot{v}_m^\infty$ is the same on either side of the future conformal boundary as the v_m is antisymmetric about this point.

If no matter were present ($\Omega_m = 0$) then we could have either symmetry in v_r if $\delta_r^\infty = 0$ or antisymmetry if $v_r^\infty = 0$. However, with the inclusion of matter, the coefficient of $\Delta\eta$ in Eq. (24) one of these channels due to the presence of terms that depend on the sign of $\Delta\eta$. The choice $v_r^\infty = 0$ automatically imposes symmetry on the remaining Eqs. (22) and (24)–(26) so we have no further quantization conditions.

These series expansions also recover the results of Ref. [5] if there is no radiation, since if $\Omega_r = 0$ then Eqs. (24) and (25) have the correct symmetry however one chooses δ_m^∞ or $\dot{v}_m^\infty$. It should also be noted that at all points $\text{sign}(\Delta\eta)$ is multiplied by Ω_m, since it is the offending $|s|^3 \neq s^3$ accompanying the material terms that prevents nonanalyticity in the expansions.

2. Anisotropic stress

As in Ref. [5], we now consider the properties of matter and radiation perturbations as they approach the future conformal boundary in the more realistic case where we do not treat radiation as a perfect fluid. To do this, we truncate Eqs. (7)–(15) so we only retain terms with $\ell \leq 2$, so our only new term is Π_r. As before, we obtain power series about the future conformal boundary. Equations (22), (24) and (25) are unchanged with the addition of anisotropic stress. Our new expansions are

$$v_r = v_r^\infty - \frac{1}{12}(3\delta_r^\infty - 2\Pi_r^\infty)\Delta\eta + \mathcal{O}(\Delta\eta^2),$$ (30)

$$\Pi_r = \Pi_r^\infty - \frac{8}{5}k^2 v_r^\infty \Delta\eta + \mathcal{O}(\Delta\eta^2),$$ (31)

$$\Phi = -\frac{3}{2k^2}\left[\text{sign}(\Delta\eta) \times H_\infty^3 \frac{\Omega_m}{\Omega_\Lambda}(\delta_m^\infty + 3\dot{v}_m^\infty) + 4H_\infty^4 \frac{\Omega_r}{\Omega_\Lambda} v_r^\infty\right]\Delta\eta + \mathcal{O}(\Delta\eta^2),$$ (32)

$$\Psi = -\frac{3}{2k^2}\left[\text{sign}(\Delta\eta) \times H_\infty^3 \frac{\Omega_m}{\Omega_\Lambda}(\delta_m^\infty + 3\dot{v}_m^\infty) + 4H_\infty^4 \frac{\Omega_r}{\Omega_\Lambda} v_r^\infty\right]\Delta\eta + \mathcal{O}(\Delta\eta^2),$$ (33)

which differ from before since the linear term of v_r now contains a correction due to anisotropic stress and the potentials now contain a term $\mathcal{O}(\Delta\eta^2)$, whereas before this was zero. It is at this order that Ψ and Φ start to disagree. We have one more equation than before, and thus one more free parameter, Π_r^∞.

Our arguments to enforce $v_r^\infty = 0$ for a perfect fluid just considered the δ_r, δ_m and v_m perturbations, whose power series have not changed to linear order. Therefore, at this order in the Boltzmann hierarchy, our quantization condition is unchanged. As before, this assertion automatically enforces symmetry or antisymmetry in Eqs. (22), (24), (25) and (30)–(33), giving us a set of allowed wave numbers with a single condition.

3. Higher-order corrections

We previously neglected the term F_{r3} in Eq. (13), so we now reintroduce this. Denoting $F_{r\ell}^\infty$ as the value of $F_{r\ell}$ at the future conformal boundary, the expansion for Π_r becomes

$$\Pi_r = \Pi_r^\infty - \frac{k}{5}(8kv_r^\infty + 9F_{r3}^\infty)\Delta\eta + \mathcal{O}(\Delta\eta^2),$$ (34)

with all other series expansions unchanged at this order. Again, the quantization condition is $v_r^\infty = 0$. However, Π_r is no longer automatically either symmetric or antisymmetric, so we would need to introduce a second quantization condition

$$\Pi_r^\infty = 0 \quad \text{or} \quad F_{r3}^\infty = 0.$$ (35)

We can generalize this to higher ℓ using Eq. (14), obtaining a further condition for each $\ell > 3$

$$\ell F_{r(\ell-1)}^\infty = (\ell + 1)F_{r(\ell+1)}^\infty \quad \text{or} \quad F_{r\ell}^\infty = 0.$$ (36)

There is no reason *a priori* why this should occur for any one k if we set each $F_{r\ell}$ to be zero at recombination, let alone for some set of these. Since $\{F_{r\ell}\}$ do not have to become nonzero at exactly the same conformal time, the freedom in $F_{r\ell}^\infty$ can be thought of as a freedom in when (near the surface of last scattering) $F_{r\ell}$ first becomes nonzero. By changing the latter the anisotropies at the FCB could be forced to have the correct symmetry.

A detailed analysis of how these initial conditions are related to each other is beyond the scope of this work, so we focus on $\ell \leq 2$ only. We refer to $\ell \leq 1$ and $\ell \leq 2$ as the "Perfect Fluid" and "Imperfect Fluid" cases respectively.

III. OBSERVATIONAL CONSEQUENCES

To compute the quantized power spectrum as detailed in the previous section we use the *Planck* 2018 best-fit parameters from the plik TTTEEE + lowl + lowE + lensing likelihoods [3] (henceforth "*Planck* baseline")
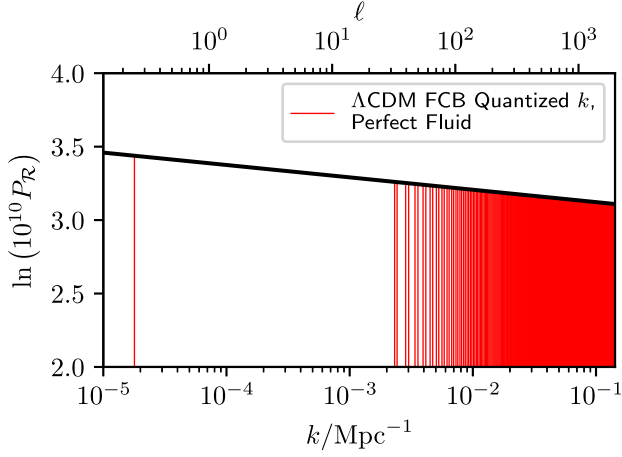
FIG. 2. Quantized primordial power spectrum $P_{\mathcal{R}}(k)$. Red vertical lines indicate the first 500 allowed comoving wave numbers k for a ΛCDM universe containing only perfect fluids with future conformal boundary quantization. Our quantization condition is that perturbations remain finite for all conformal times.

for H_0, Ω_Λ, Ω_m and Ω_r. We integrate our background equations using LSODA from scipy.integrate.solve_ivp [10] with relative and absolute precision of 10^{-13}. The resulting background is used to solve for perturbations up to recombination by integrating Eqs. (3)–(5). We set $\Phi = \Psi$ at recombination and let this equal the potential from the perfect fluid integration. Likewise, the density and velocity perturbations are assumed to be continuous at recombination and we set $\Pi_r = 0$ at this point. We now integrate Eqs. (7)–(13) for $\ell \leq 2$ from recombination up to the future conformal boundary and find the perturbations which satisfy $v_r^\infty = 0$ via a root-finding algorithm.

The first three allowed perturbations are plotted in Fig. 1 for a perfect fluid. For numerical stability, we solve for $\log a$ instead of a at small conformal times.

The quantized primordial power spectrum in the perfect fluid approximation is shown graphically[1] for the first 500 allowed wave numbers in Fig. 2.

In Fig. 3 we plot the radiation velocity perturbation at the FCB and indicate the allowed wave numbers at the zeros of v_r^∞. We see that the spacing is initially nonlinear, but, like in the pure radiation case, the wave numbers quickly settle down to linear. A linear fit to the allowed wave numbers $k/\sqrt{\Lambda} \leq 10$ yields a smallest two allowed wave numbers of

$$k_0^{\text{perfect}} = 0.056\sqrt{\Lambda} = 1.79 \times 10^{-5} \text{ Mpc}^{-1}, \quad (37)$$

---

[1]Throughout this paper we use an approximate conversion between k and ℓ via the Limber approximation [11] $\ell \sim kD_A$ where D_A is the comoving angular diameter distance to last scattering. This is a parameter-dependant conversion so for consistency we use the *Planck* 2018 ΛCDM baseline cosmological parameters from Ref. [3] to define this transformation.
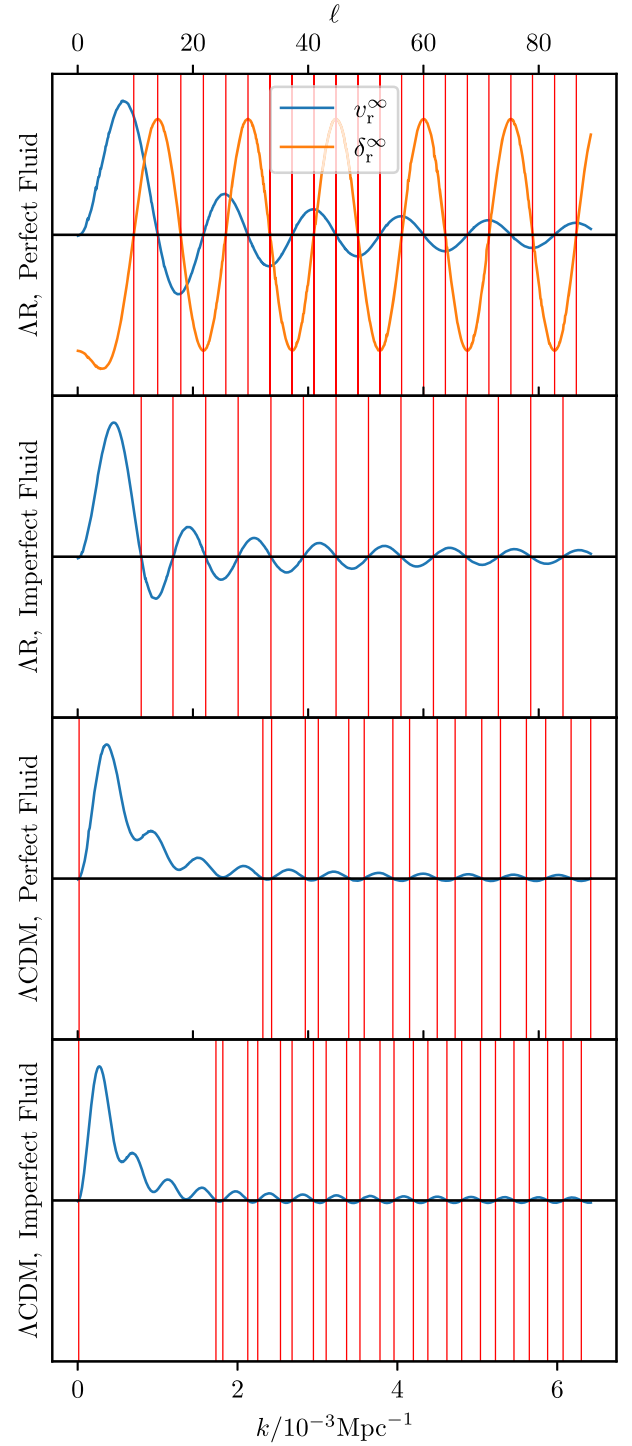

FIG. 3. Radiation velocity perturbation evaluated at the future conformal boundary, v_r^∞, as a function of comoving wave number k for a ΛR and a ΛCDM universe with *Planck* baseline parameters. The perturbations associated with a given k remain finite for all conformal times at the wave numbers shown with red lines. Note that the ΛR cosmology containing only perfect fluids does not have an allowed mode at the first zero of v_r^∞ [5]. For this case we also plot the radiation density perturbation at the future conformal boundary, δ_r^∞, since in this case $\delta_r^\infty = 0$ is also a permitted quantization condition.

$$k_1^{\text{perfect}} = 7.22\sqrt{\Lambda} = 2.32 \times 10^{-3} \text{ Mpc}^{-1}, \qquad (38)$$

and asymptotic spacing

$$\Delta k^{\text{perfect}} = 0.877\sqrt{\Lambda} = 2.82 \times 10^{-4} \text{ Mpc}^{-1}, \quad (39)$$

for the perfect fluid, and

$$k_0^{\text{imperfect}} = 0.042\sqrt{\Lambda} = 1.34 \times 10^{-5} \text{ Mpc}^{-1}, \quad (40)$$

$$k_1^{\text{imperfect}} = 5.39\sqrt{\Lambda} = 1.73 \times 10^{-3} \text{ Mpc}^{-1}, \quad (41)$$

$$\Delta k^{\text{imperfect}} = 0.657\sqrt{\Lambda} = 2.11 \times 10^{-4} \text{ Mpc}^{-1}, \quad (42)$$

when we include the effects of anisotropic stress.

As expected, since v_r has an oscillatory complementary function near the FCB which varies as $\sim \cos{(k\eta/\sqrt{3})}$, the spacing should be approximately $\Delta k = \sqrt{3}\pi/\eta_{\text{fcb}} = 2.82 \times 10^{-4} \text{ Mpc}^{-1}$, which is consistent with the numerically calculated value of the perfect fluid case.

We note three differences in comparison with the pure radiation case:

(i) The introduction of matter dramatically decreases the infrared cutoff since we do not have to exclude the $k/\sqrt{\Lambda} = \sqrt{2}$ mode.

(ii) The inclusion of matter creates "missing" modes; there are local minima in v_r^{∞} which do not have roots of $v_r^{\infty} = 0$ between them. This results in k_1 for ΛCDM universes being much larger than the first few allowed modes of ΛR universes. This is illustrated in Fig. 1, where we see that the radiation density and velocity perturbations for the $n = 1$ mode exhibit many cycles of oscillation before the FCB, although one would naively expect just one given the shape of the $n = 0$ mode.
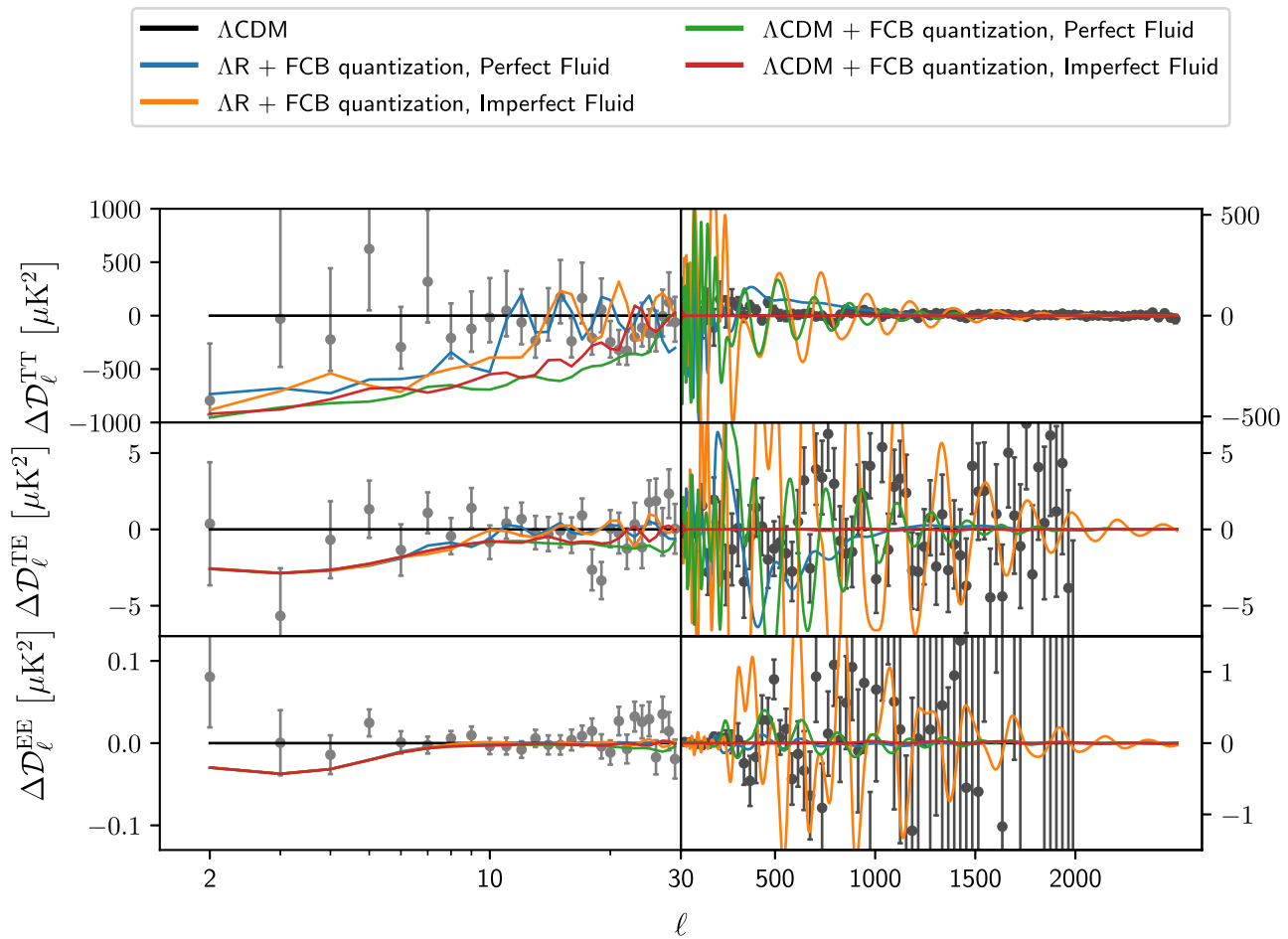

FIG. 4. CMB power spectrum residuals between future conformal boundary quantized cosmologies and the ΛCDM baseline. ΛCDM + FCB quantization is in red and green, while ΛR + FCB is in blue and orange. The *Planck* data residuals are also plotted for reference. The quantized cosmologies only allow comoving wave numbers k such that perturbations remain finite for all conformal times. This restriction results in a drop in power at low ℓ due to a minimum allowed k_0 (and a corresponding rise at k_0) and oscillatory features from the finite spacing Δk between allowed wave vectors. The cosmological parameters for all models are fixed to the *Planck* baseline values.
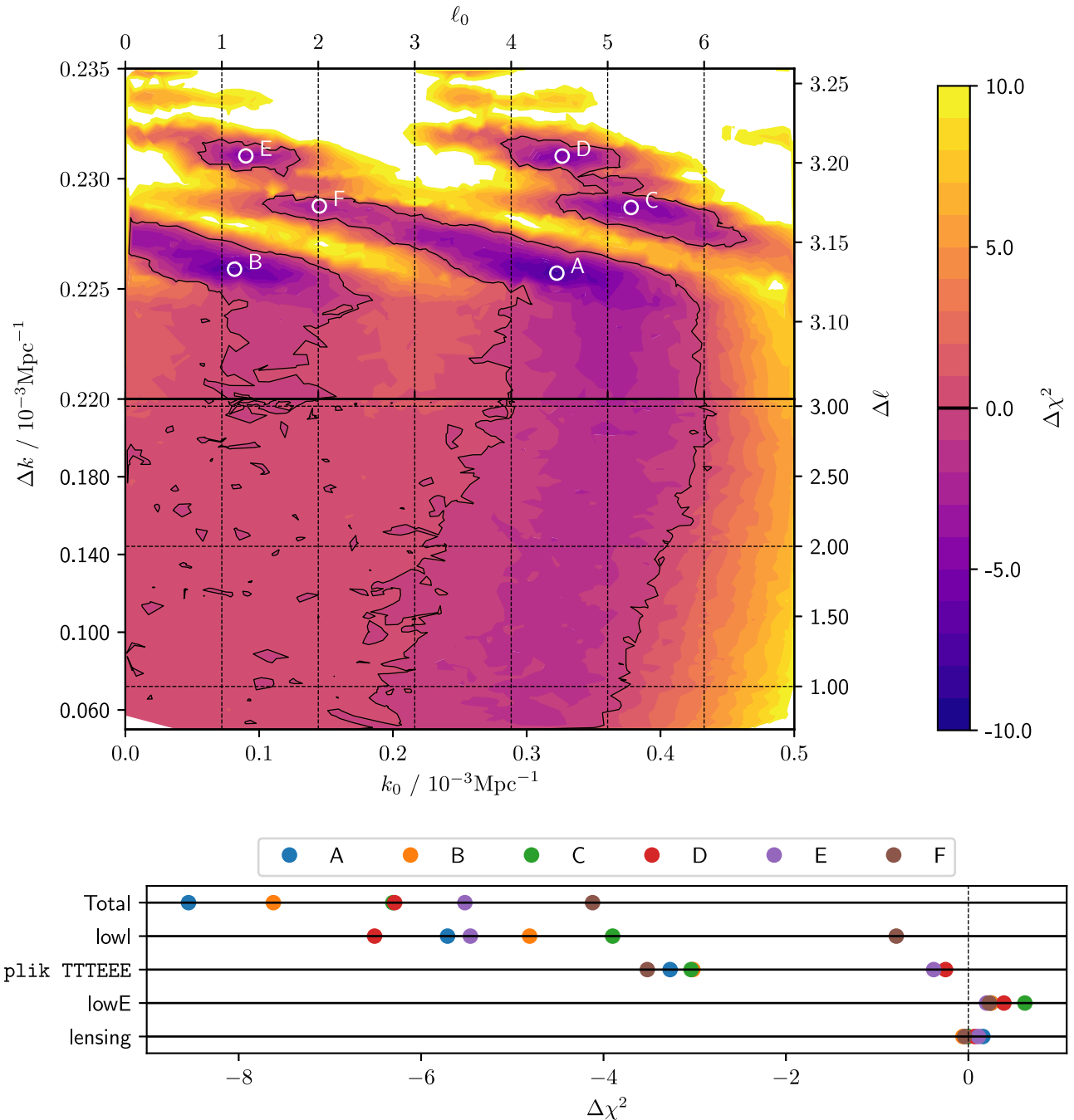
FIG. 5. Upper: profile likelihood plot showing the difference of quality of fit $\Delta\chi^2$ between linearly quantized and ΛCDM models as a function of the first allowed comoving wave number k_0 and spacing Δk optimized over all other cosmological and nuisance parameters. Negative $\Delta\chi^2$ indicates a better fit for the quantized model. The best-fit point (A) has $\chi^2 = 2759.34$ which corresponds to $\Delta\chi^2 = -8.55$. The plot was produced by exploiting the embarrassingly parallel nature of the problem by randomly choosing $(k_0, \Delta k)$ pairs, then optimizing over all other cosmological and nuisance parameters, which accounts for the small amount of noise in the contours. Lower: improvement in χ^2 is driven by the reduction in lowl, although there is intriguingly also an improved high-ℓ contribution.

(iii) We only allow half the modes as in the perfect fluid radiation case (just the zeros of v_r^∞ as opposed to both the zeros and turning points). However, since η_{FCB} is approximately twice as large in the ΛCDM case, the spacing is almost unchanged.

Due to the linearity at high n, we will explicitly calculate the allowed wave numbers for $k/\sqrt{\Lambda} \leq 10$, and then extrapolate to produce a complete spectrum.

To investigate the observational consequences of FCB quantization, we compute the predicted C_ℓ spectra using a

TABLE I. Cosmological and nuisance parameters which optimize χ^2 for a linearly quantized k spectrum. The parameter shifts between the quantized spectrum and the ΛCDM baseline are given in terms of the posterior parameter widths σ [3].

Parameter	Best-fit value	Change/σ
$\Omega_b h^2$	0.022279	-0.36
$\Omega_c h^2$	0.12031	0.04
$100\theta_{\mathrm{MC}}$	1.041871	0.14
$\ln\left(10^{10} A_s\right)$	3.0380	-0.01
n_s	0.96067	-0.66
τ	0.0529	0.10
y_{cal}	1.00071	0.22
A_{217}^{CIB}	45.5	-0.20
$\xi^{tSZ-CIB}$	0.60	0.86
A^{tSZ}	8.69	0.58
A_{100}^{PS}	195.7	-1.23
A_{143}^{PS}	28.0	-1.00
$A_{143\times217}^{PS}$	35.8	-0.18
A_{217}^{PS}	106.2	-0.60
A^{kSZ}	9.763	2.08
A_{100}^{dustTT}	7.65	0.08
A_{143}^{dustTT}	17.00	1.66
$A_{143\times217}^{dustTT}$	24.83	1.03
A_{217}^{dustTT}	99.1	0.37
A_{100}^{dustTE}	0.02	-0.95
$A_{100\times143}^{dustTE}$	0.12	0.26
$A_{100\times217}^{dustTE}$	0.53	-0.25
A_{143}^{dustTE}	0.279	1.00
$A_{143\times217}^{dustTE}$	0.66	-0.17
A_{217}^{dustTE}	2.202	-0.20
c_{100}	0.99689	-1.90
c_{217}	0.99738	-0.81
$k_0/10^{-3}\ \mathrm{Mpc}^{-1}$	0.3225	…
$\Delta k/10^{-3}\ \mathrm{Mpc}^{-1}$	0.2257	…

modified version of CLASS [12], changed to allow primordial power spectra with a discrete rather than continuous set of wave numbers (for more details, see the Appendix). We implement this by adapting parts of the code traditionally used for closed universes since these also have a quantized spectrum. We initially consider five cases:

 (i) The traditional ΛCDM power spectrum.
 (ii) The quantized power spectrum arising from future conformal boundary considerations for a ΛCDM universe using the perfect fluid approximation.
 (iii) The quantized power spectrum arising from future conformal boundary considerations for a ΛCDM universe where we include the effects of anisotropic stress.
 (iv) The quantized power spectrum arising from future conformal boundary considerations for a ΛR universe from Ref. [5], using the perfect fluid approximation.
 (v) The quantized power spectrum arising from future conformal boundary considerations for a ΛR universe from Ref. [5], where we include the effects of anisotropic stress.

Assuming the *Planck* baseline cosmological parameters, the power spectral differences between ΛCDM and the quantized cosmologies are plotted in Fig. 4 alongside the *Planck* residuals. There are two main features observed in all three plots. The first is a drop in power at low ℓ, which is to be expected since there exists a minimum allowed k in our quantized cosmology. We find k_0 corresponds to $\ell_0 < 1$ for ΛCDM FCB quantization, whereas k_1 corresponds to $\ell_1 = 32$ for the perfect fluid, and $\ell_1 = 24$ for the imperfect case. This explains why we see smaller values of $\mathcal{D}_\ell$ for $\ell \lesssim 30$, but no rise in power at the smallest ℓ, and thus the effective infrared cutoff can be considered to be k_1 in this scenario. The absence of the $k/\sqrt{\Lambda} = \sqrt{2}$ mode for a ΛR cosmology of perfect fluids explains the lack of the rise in that case and can therefore account for the low quadrupole [13] of the TT and octupole of the TE spectrum. The second disparity between the two cosmologies is an oscillatory behavior at all ℓ values due to the spacing between allowed k values.

It is clear that these infrared cutoffs are implausible for both the ΛCDM and ΛR cases, and completely ruled out by
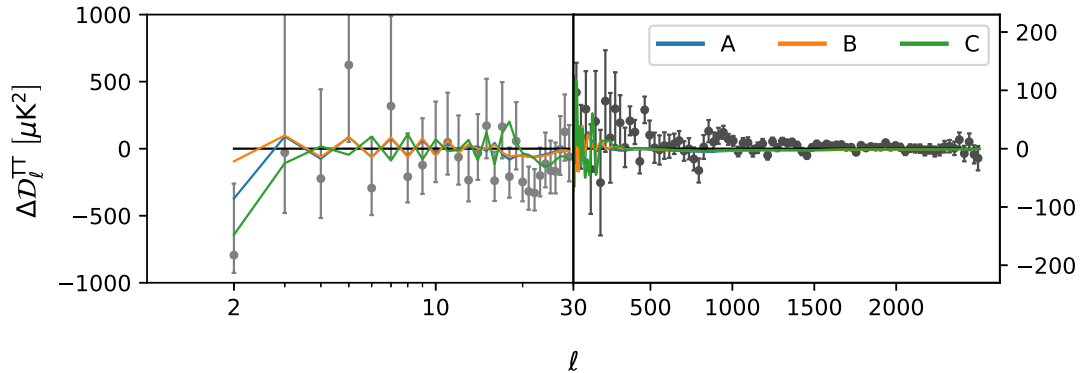

FIG. 6. CMB temperature residuals between the best-fitting linearly quantized cosmologies and the *Planck* baseline ΛCDM model, fitted using the full *Planck* baseline likelihood. Each of the lines correspond to the three best-fitting points from Fig. 5. Our quantization condition introduces a drop in power at low ℓ and a dip at $20 \lesssim \ell \lesssim 30$.

modern cosmological observations. To test this, we use parameters from the *Planck* posterior samples [14] and find that we cannot obtain cosmological parameters which give a nonzero likelihood for the predicted CMB power spectra. We compute the first two allowed k values for all parameters from the *Planck* posterior samples, and find that the smallest value of ℓ_1 is 30.5 for a perfect fluid, and 22.8 for the imperfect case. As will become apparent in Sec. IV, these are too high to allow reasonable low-ℓ behavior, although the Δk obtained could be acceptable if more modes were allowed between k_0 and k_1. Since the imperfect fluid produced a smaller k_1 than the perfect fluid approximation, in future work we will investigate the effects of including higher-order terms in the Boltzmann hierarchy and more sophisticated modeling of recombination on the quantized primordial power spectrum, as this may reintroduce the "missing" modes in Fig. 3.

IV. LINEAR QUANTIZATION IN GENERAL

Although FCB quantization does not provide quantitatively good fits to CMB power spectra, the previous section demonstrated that a quantized k spectrum produces qualitatively interesting features such as a drop in power at low ℓ and a dip at $20 \lesssim \ell \lesssim 30$. Since the ΛR and ΛCDM FCB quantized spectra become linearly spaced at large k, we now consider whether a more general quantized, linearly spaced k spectrum can provide a better fit to the *Planck* data.

To do this, we introduce a finite spacing between allowed wave numbers Δk and a minimum allowed k value k_0 such that

$$k_n = k_0 + n\Delta k, \quad n = 0, 1, 2\ldots \tag{43}$$

where we treat k_0 and Δk as free parameters.

The profile likelihood plot conditioned on k_0 and Δk with the remaining parameters minimized over is shown in Fig. 5. We optimize using the Nelder-Mead algorithm [15]

with a simplex consisting of the parameters within the *Planck* posterior samples with the highest likelihood.

For small Δk (for which $\Delta \ell \lesssim 1$ and thus the spacing between k values is negligible), we see that we can achieve a marginally better fit than the ΛCDM case if $k_0 \sim 3 \times 10^{-4}$ Mpc^{-3}. This is consistent with previous studies [16,17] which found that introducing an infrared cutoff can slightly improve the low-ℓ predictions.

The six labeled points (A–F) are local minima in χ^2. The resulting χ^2 and its contributions for these points are also shown in Fig. 5. All these points have $\Delta \ell \gtrsim 3.1$, and thus we find that introducing a nontrivial finite spacing between k values can significantly improve the value of χ^2, by up to -8.55. As expected, this is driven by an improvement in lowl, although there is also a noticeable improvement in the high-ℓ likelihoods. The best-fit point (A) resides at

$$k_0 = 3.225 \times 10^{-4} \text{ Mpc}^{-1}, \tag{44}$$

$$\Delta k = 2.257 \times 10^{-4} \text{ Mpc}^{-1}. \tag{45}$$

The cosmological and nuisance parameters which provide this best fit are given in Table I, which are not significantly changed from the ΛCDM baseline [3]. The cosmological parameters are all consistent with those from the ΛCDM case; however the nuisance parameters shift a little more, but still at $\lesssim 2\sigma$.

In Fig. 6 we plot the CMB TT power spectra for points A–C. From this we identify the improvement as being due to a reduced quadrupole compared to the ΛCDM case and a dip following the *Planck* data at $20 \lesssim \ell \lesssim 30$. The TE and EE spectra are not shown as the differences between the quantized and ΛCDM cases are negligible for these spectra.

The best-fit cutoff corresponds to $\ell_0 \sim 4.5$, compared to $\ell_1^{(\Lambda\text{CDM})} \sim 32$ and $\ell_0^{(\Lambda\text{R})} \sim 9.7$ for our FCB quantized models. Since the spacing Δk is comparable for all our quantizations, we see that the reason for the poor fit in the future conformal boundary models is the large infrared cutoff. This resulted in a decrease in CMB power at too
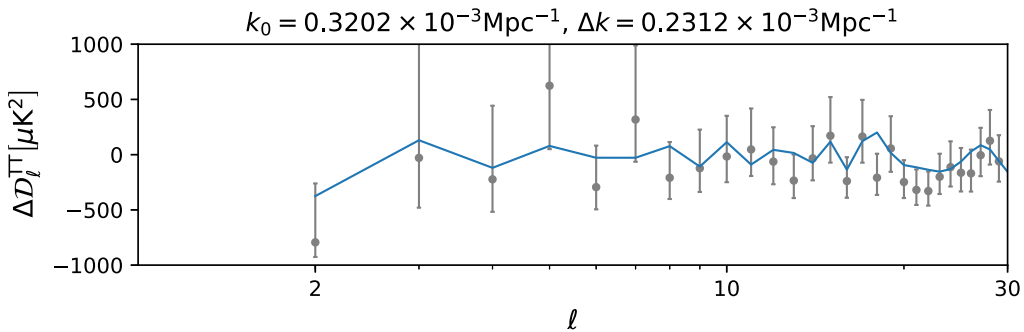

FIG. 7.   CMB temperature residuals between the best-fit linearly quantized cosmology and the *Planck* baseline ΛCDM model, fitted using just the lowl likelihood. Cosmological and nuisance parameters were fixed to the ΛCDM baseline. The best-fit k_0 and Δk give Δlowl $= -6.97$. Without the influence of the high-ℓ likelihood, linearly quantized cosmologies are able to more accurately fit the $20 \lesssim \ell \lesssim 30$ dip.
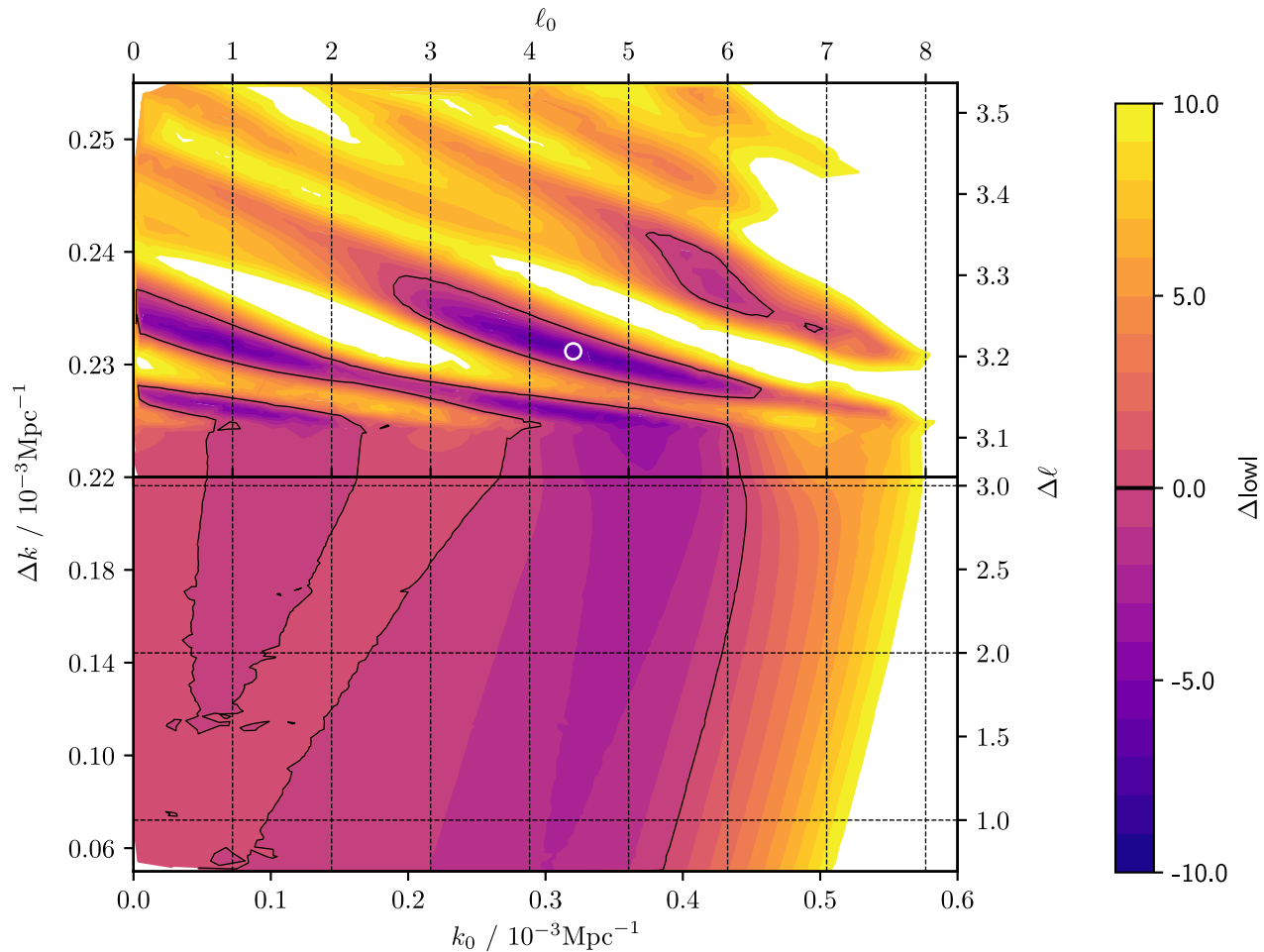
FIG. 8. Difference of quality of fit Δlowl between linearly quantized and ΛCDM models as a function of the first allowed comoving wave number k_0 and spacing Δk, where the cosmological and nuisance parameters are fixed to the ΛCDM baseline. Negative Δlowl indicates a better fit for the quantized model. The best-fit point (circled) has lowl $= 16.57$ which corresponds to Δlowl $= -6.97$.

high a multipole, but from Fig. 6 we see that a drop in power at $\ell \sim 4.5$ provides a far more reasonable spectrum.

Since lowl dominates the improvement in χ^2, it is informative to consider optimizing over just lowl, fixing the remaining cosmological parameters to the *Planck* baseline. In doing so we obtain the CMB TT power spectra plotted in Fig. 7 and obtain a still stronger improvement of Δlowl $= -6.97$, with the improvement driven by an enhanced $20 \lesssim \ell \lesssim 30$ feature. We show how lowl varies with k_0 and Δk in Fig. 8.

V. CONCLUSIONS

In this paper, in Sec. II we extended the results of Ref. [5] to account for universes which simultaneously include radiation, cold dark matter and a cosmological constant, showing that both models produce similar quantized primordial power spectra. In Sec. III we examined the observational implications of these models, and found them to produce qualitatively interesting features in the cosmic

microwave background power spectrum, namely a suppression of power at low ℓ, a dip at $20 \lesssim \ell \lesssim 30$ and oscillations at high ℓ. Quantitatively however, these models do not produce CMB power spectra consistent with modern cosmological observations. Inspired by the qualitatively interesting features generated by these quantized power spectrum models, in Sec. IV we examined a wider class of linearly quantized models with quantized wave vectors $\{k_0 + n\Delta k : n = 0, 1, \ldots\}$. In this case we found that for values of $(k_0, \Delta k) = (3.225, 2.257) \times 10^{-4} \; \mathrm{Mpc}^{-1}$ these quantized primordial power spectra give markedly improved fits in comparison with the baseline concordance cosmological model, with $\Delta\chi^2 = -8.55$. To a large extent this improvement is driven by the lowl likelihood, and when optimized only using lowl without the influence of high-ℓ likelihoods on the fit, one can extract a Δlowl $= -6.97$.

It should be noted that while the results for linearly quantized primordial power spectra are interesting, far

more work needs to be done before these can be considered feasible cosmological models. The Δk parameter is highly fine-tuned, with the region of best-fit occupying roughly one percent of any reasonable prior. If these models were to be subject to a Bayesian analysis with evidences and parameter estimation [18] there would be a subsequent Occam penalty which would penalize the quality of the fit. These results are also profiled, and sampling over the full parameter space would also degrade the quality of the fit. However, if there were models akin to the future conformal boundary quantizations that predicted *a priori* a quantized primordial power spectrum with $\Delta k \sim 2.257 \times 10^{-4}$ Mpc^{-1}, then these likelihood results suggest that these models would be candidates for a new concordance cosmology. In future work we will extend the future conformal boundary models to include higher-order multipoles in the Boltzmann hierarchy and a more sophisticated treatment of recombination to determine whether this class of models could achieve this.

There is also no need for these quantizations to be linearly spaced across the observable window. The fact that one can extract better low-ℓ fits by ignoring the high-ℓ likelihood suggests that if Δk varied with k still better fits might be obtained. There is also potential for using a free-form reconstruction approach [19] to determine the optimal locations and numbers of quantized wave vectors.

It is clear that there are many theoretical, observational and reconstructive investigations required into models with quantized primordial power spectra, but this work shows that there is compelling observational evidence for increased research effort into these cosmologies.

ACKNOWLEDGMENTS

APPENDIX: POWER SPECTRA WITH QUANTIZED k

In this Appendix we follow the derivations given in Ref. [21], but adapted for a quantized spectrum.

Consider some function $f(\vec{x}, \hat{n}, \eta)$. Since a continuous spectrum of comoving wave numbers $k = |\vec{k}|$ is usually assumed in perturbation analysis, the canonical definitions for various quantities of interest are defined in terms of integrals. We must therefore rewrite our fields as Fourier series, defined as

$$f(\vec{x}, \hat{n}, \eta) = \sum_k k^2 \Delta k \int d\Omega_k e^{i\vec{k}\cdot\vec{x}} f(\vec{k}, \hat{n}, \eta), \quad (A1)$$

where Ω_k denotes the solid angle in k space, we are looking in the direction of the unit vector $\hat{n}$ and where η is conformal time $d\eta \equiv a dt$ for scale factor $a(\eta)$ with cosmic time t.

We introduced the spacing $\Delta k(k)$ between allowed wave numbers $k = |\vec{k}|$ as a weighting to our Fourier coefficients so that all variables have the same dimensions as in the continuous case.

At the origin $(\vec{x} = \vec{0})$,

$$f(\hat{n}) = \sum_{\ell=0}^{\infty} \sum_{m=-\ell}^{\ell} a_{\ell m} Y_{\ell m}(\hat{n}), \quad (A2)$$

where, by orthogonality,

$$a_{\ell m} = \int d\Omega f(\hat{n}) Y_{\ell m}^*(\hat{n}). \quad (A3)$$

Expanding in terms of Legendre polynomials,

$$f(\vec{x}, \hat{n}, \tau) = \sum_k k^2 \Delta k \int d\Omega_k \sum_{\ell=0}^{\infty} (-i)^\ell (2\ell + 1) e^{i\vec{k}\cdot\vec{x}} \\ \times f_\ell(\vec{k}, \tau) P_\ell(\hat{k} \cdot \hat{n}), \quad (A4)$$

and using the identity

$$P_{\ell'}(\hat{k} \cdot \hat{n}) = \frac{4\pi}{2\ell' + 1} \sum_{m'} Y_{\ell' m'}^*(\hat{k}) Y_{\ell' m'}(\hat{n}), \quad (A5)$$

we obtain

$$a_{\ell m} = (-i)^\ell 4\pi \sum_k k^2 \Delta k \int d\Omega_k Y_{\ell m}^*(\hat{k}) f_\ell(\vec{k}, \tau). \quad (A6)$$

We now define

$$f_\ell(\vec{k}, \tau) \equiv \psi_i(\vec{k}) f_\ell(k, \tau), \quad (A7)$$

since the evolution equations are independent of $\hat{k}$, where $\psi_i(\vec{k})$ is the initial perturbation and $f_\ell(k, \tau)$ is the photon transfer function in the case $f(\vec{x}, \hat{n}, \tau) = \Delta(\vec{x}, \hat{n}, \tau)$.

We define

$$\langle \psi_i(\vec{k})\psi_i(\vec{k}') \rangle \equiv P_\psi(k) \frac{\delta^{(K)}_{kk'}}{k^2 \Delta k} \delta^{(D)}(\hat{k} + \hat{k}'), \quad \text{(A8)}$$

where $\delta^{(K)}_{ab}$ is the Kronecker delta, and $\delta^{(D)}(\vec{a} - \vec{b})$ is the Dirac delta function. As before, the Δk is introduced in the definition to be dimensionally consistent with the continuous case. We also define the power spectrum to be

$$\langle a_{\ell m} a^*_{\ell' m'} \rangle \equiv C_\ell \delta^{(K)}_{\ell \ell'} \delta^{(K)}_{mm'}, \quad \text{(A9)}$$

and therefore

$$C_\ell = (4\pi)^2 \sum_k k^2 \Delta k P_\psi(k) f_\ell^2(k, \tau). \quad \text{(A10)}$$

Consequently, we can summarize the continuous to quantized crossover as "replace by a sum," where we mean

$$\int (\cdots) \, dk \to \sum_k (\cdots) \Delta k, \quad \text{(A11)}$$

when we wish to convert an expression defined with a continuous k spectrum to one with a quantized spectrum.

As usual, C_ℓ is related to $\mathcal{D}_\ell$ as

$$\mathcal{D}_\ell \equiv \frac{\ell(\ell + 1)}{2\pi} C_\ell. \quad \text{(A12)}$$

Since the basis $e^{i\vec{k}\cdot\vec{x}}$ is orthogonal irrespective of whether we do an integral or sum, we solve the same equations for perturbations as in the continuous case.

One caveat of introducing the summation instead of an integral is that, when deriving the curvature perturbations from inflation, we cannot use a completeness relation when quantizing the inflaton. Instead of dwelling on this, we assume an initially (nearly) scale-invariant power spectrum,

$$\mathcal{P}_\mathcal{R}(k) = A_s k^{n_s - 1}, \quad \text{(A13)}$$

without concern over its origin.

[1] C. L. Bennett *et al.*, Nine-year Wilkinson Microwave Anisotropy Probe (WMAP) Observations: Final Maps and Results, Astrophys. J. Suppl. Ser. **208,** 20 (2013).

[2] *Planck* Collaboration, *Planck* 2013 results. XVI. Cosmological parameters, Astron. Astrophys. **571,** A16 (2014).

[3] *Planck* Collaboration, *Planck* 2018 results. VI. Cosmological parameters, Astron. Astrophys. **641,** A6 (2020).

[4] J. Chluba, J. Hamann, and S. P. Patil, Features and new physical scales in primordial observables: Theory and observation, Int. J. Mod. Phys. D **24,** 1530023 (2015).

[5] A. N. Lasenby, W. J. Handley, D. J. Bartlett, and C. S. Negreanu, preceding paper, Perturbations and the future conformal boundary, Phys. Rev. D **105,** 083514 (2022).

[6] L. Boyle and N. Turok, Two-Sheeted Universe, Analyticity and the Arrow of Time, arXiv:2109.06204.

[7] *Planck* Collaboration, Planck 2018 results. V. CMB power spectra and likelihoods, Astron. Astrophys. **641,** A5 (2020).

[8] *Planck* Collaboration, *Planck* 2018 results. VIII. Gravitational lensing, Astron. Astrophys. **641,** A8 (2020).

[9] C.-P. Ma and E. Bertschinger, Cosmological perturbation theory in the synchronous and conformal newtonian gauges, Astrophys. J. **455,** 7 (1995).

[10] E. Jones, T. Oliphant, P. Peterson *et al.*, SciPy: Open source scientific tools for PYTHON, 2001, http://www.scipy.org/.

[11] P. Lemos, A. Challinor, and G. Efstathiou, The effect of Limber and flat-sky approximations on galaxy weak lensing, J. Cosmol. Astropart. Phys. 05 (2017) 014.

[12] D. Blas, J. Lesgourgues, and T. Tram, The cosmic linear anisotropy solving system (CLASS). Part II: Approximation schemes, J. Cosmol. Astropart. Phys. 07 (2011) 034.

[13] A. Iqbal, J. Prasad, T. Souradeep, and M. A. Malik, Joint Planck and WMAP assessment of low CMB multipoles, J. Cosmol. Astropart. Phys. 06 (2015) 014.

[14] Planck Collaboration, Planck legacy archive, https://pla.esac.esa.int, 2019 (Accessed: 2019-02-10).

[15] F. Gao and L. Han, Implementing the nelder-mead simplex algorithm with adaptive parameters, Comput. Optim. Applic. **51,** 259 (2012).

[16] Y.-P. Jing and L.-Z. Fang, An Infrared Cutoff Revealed by the Two Years of COBE—DMR Observations of Cosmic Temperature Fluctuations, Phys. Rev. Lett. **73,** 1882 (1994).

[17] R. Sinha and T. Souradeep, Post-wmap assessment of infrared cutoff in the primordial spectrum from inflation, Phys. Rev. D **74,** 043518 (2006).

[18] R. Trotta, Bayes in the sky: Bayesian inference and model selection in cosmology, Contemp. Phys. **49,** 71 (2008).

[19] W. J. Handley, A. N. Lasenby, H. V. Peiris, and M. P. Hobson, Bayesian inflationary reconstructions from *Planck* 2018 data, Phys. Rev. D **100,** 103511 (2019).

[20] http://www.esa.int/Planck.

[21] C.-P. Ma and E. Bertschinger, Cosmological perturbation theory in the synchronous and conformal Newtonian gauges, Astrophys. J. **455,** 7 (1995).